Nano Energy 60 (2019) 545–556

Contents lists available at ScienceDirect

Nano Energy

journal homepage: www.elsevier.com/locate/nanoen

Full paper

Triboelectric single-electrode-output control interface using patterned grid electrode

Qiongfeng Shi[a,b,c,d], Chunkai Qiu[e], Tianyiyi He[a,b,c,d], Fan Wu[e], Minglu Zhu[a,b,c,d], Jan A. Dziuban[f], Rafał Walczak[f,***], Mehmet Rasit Yuce[e,**], Chengkuo Lee[a,b,c,d,g,*]

[a] Department of Electrical and Computer Engineering, National University of Singapore, 4 Engineering Drive 3, 117576, Singapore
[b] Center for Intelligent Sensors and MEMS, National University of Singapore, Block E6 #05-11, 5 Engineering Drive 1, 117608, Singapore
[c] Hybrid-Integrated Flexible (Stretchable) Electronic Systems Program, National University of Singapore, Block E6 #05-3, 5 Engineering Drive 1, 117608, Singapore
[d] NUS Suzhou Research Institute (NUSRI), Suzhou Industrial Park, Suzhou, 215123, PR China
[e] Department of Electrical and Computer Systems Engineering, Monash University, Melbourne, VIC, 3800, Australia
[f] Faculty of Microsystem Electronics and Photonics, Wroclaw University of Science and Technology, 11/17 Janiszewskiego Street, Wroclaw, 50-372, Poland
[g] NUS Graduate School for Integrative Science and Engineering, National University of Singapore, 117456, Singapore

ARTICLE INFO

Keywords:
Control interface
Triboelectric
Single electrode
Self-powered
Patterned grid

ABSTRACT

Control interfaces are important devices for connecting human with machines to achieve various manipulations. Recently, the emerging triboelectric based control interfaces exhibit great advantages in flexible wearable and battery-less applications. To further reduce the device complexity and improve the device practicability, a minimalist control interface with only one sensing electrode is developed based on sliding triboelectric mode. The developed control interface consists of connected grid metal pattern as single-electrode output for multi-directional sensing and controlling. This design provides superior advantages, including realization of multi-directional sensing and controlling using only one electrode and ultra-robust detection mechanism based on the number of the generated output peaks. Compared to the traditional triboelectric nanogenerators, this detection mechanism only depends on the number of the output peaks rather than the absolute magnitude, offering high robustness and reliability in various usage scenarios and for different users. Based on the minimalist design, two types of devices are proposed for the applications of 2D and 3D control. First, a flexible 2D-control patch with single electrode is developed to achieve in-plane 2D control. Next, through the integration of two similar patches on both sides of a card, a flexible 3D-control card is achieved to realize 3D control. In addition, the control patch and the control card are then investigated in terms of energy harvesting performance, both of which show good performance in scavenging energy from human tapping. In practical usage, these two devices are successfully demonstrated for 2D vehicle control and 3D virtual drone control, respectively. The developed flexible, self-powered and minimalist control interfaces exhibit promising potentials for diverse applications such as gaming, virtual/augmented reality, entertainment, smart home, and robotics control, etc.

1. Introduction

Modern society has witnessed the blooming prosperity of internet-of-things (IoT) devices in both industry and personal electronics. In the next few years, it is predicted that the total number of IoT devices will experience explosion growth on earth [1]. Among the huge number of IoT devices, flexible wearable electronics have received tremendous attention with broad applications in human motion tracking and physiological signal monitoring [2–8]. Traditional flexible wearable sensors are normally developed based on resistive [9], capacitive [10], or piezoelectric mechanism [11,12], in order to perform detection and sensing. Recently, flexible wearable devices with self-powered capability are of great importance to address the increasing energy crisis and enable battery-less applications. Triboelectric nanogenerator (TENG) based on the coupling of contact electrification and electrostatic induction has been demonstrated as a promising energy

* Corresponding author. Department of Electrical and Computer Engineering, National University of Singapore, 4 Engineering Drive 3, 117576, Singapore.
** Corresponding author. Department of Electrical and Computer Systems Engineering, Monash University, Melbourne, VIC, 3800, Australia.
*** Corresponding author. Faculty of Microsystem Electronics and Photonics, Wroclaw University of Science and Technology, 11/17 Janiszewskiego Street, Wroclaw, 50-372, Poland.
E-mail addresses: rafal.walczak@pwr.edu.pl (R. Walczak), mehmet.yuce@monash.edu (M.R. Yuce), elelc@nus.edu.sg (C. Lee).

https://doi.org/10.1016/j.nanoen.2019.03.090
Received 7 February 2019; Received in revised form 14 March 2019; Accepted 27 March 2019
Available online 30 March 2019
2211-2855/

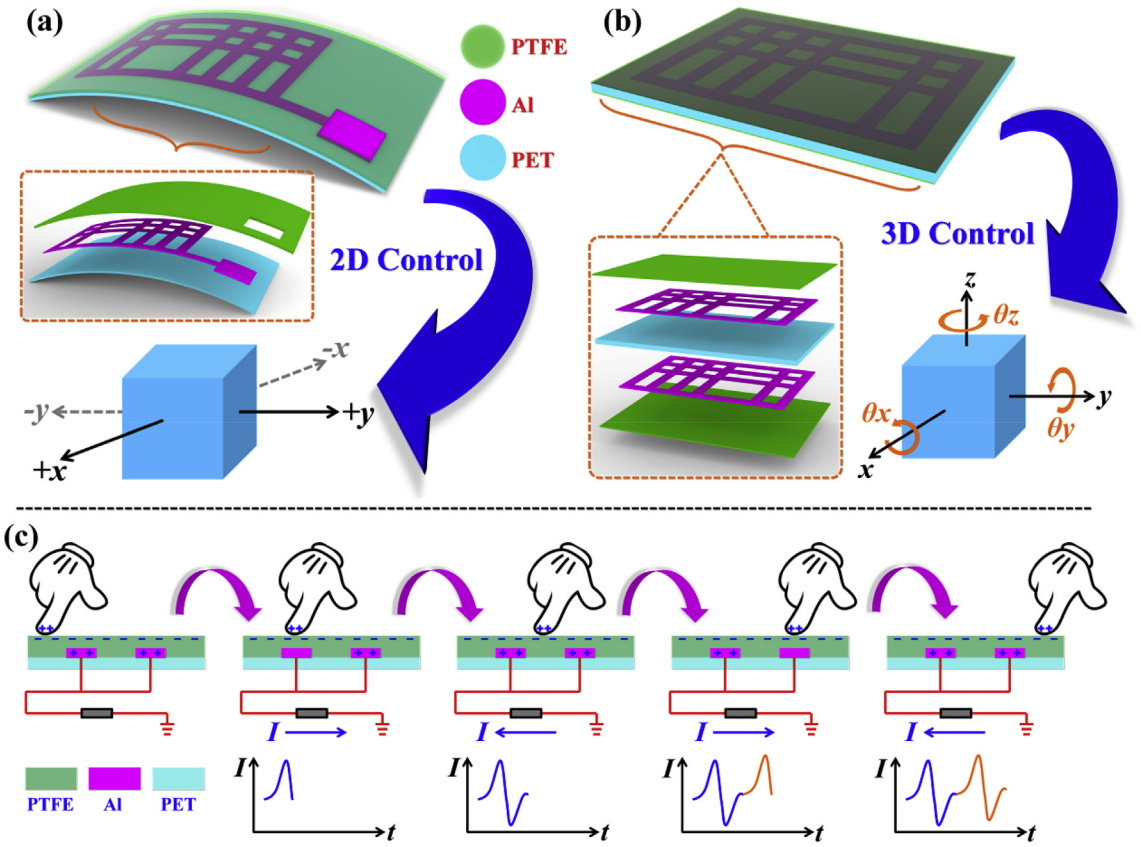

Fig. 1. Device schematics and operation mechanism. (a) The flexible control patch and its application in 2D control. (b) The portable control card and its application in 3D control. (c) Operation mechanism of sliding across the grating electrodes for output signal generation.

harvesting technology since its first invention in 2012 by Prof. Z.L. Wang and his team [13–20]. The developed TENG technology exhibits great advantages toward wearable and battery-less applications including self-generated signals and ultra-wide material choice. Thereafter, significant research efforts have been stimulated across the world [21–32], showing rapid development in diverse application areas such as energy harvesters [33–43], self-powered sensors and actuators [44–48]. To collect and use different types of random energy in the environment more effectively, hybridized TENGs are developed to scavenge and store multiple types of energy including mechanical, solar energy, thermal and chemical energy [49–53].

Control interface is important interfacing component between the interaction of human and machine. Along with the rapid development of TENGs, triboelectric control interfaces have also attracted increasing interest, with unique advantages of self-generated signals, high performance, flexible or even stretchable property, no limitation in material, and low cost. Previously reported triboelectric control interfaces are normally based on contact-separation (CS) mode [54] or lateral-sliding (LS) mode [55]. CS mode based devices generally consist of two separated friction layers with respective electrodes, which are integrated together with spacer in-between. If under external pressure such as pressing, the two friction layers will come into contact and generate current flow in the external circuit. In terms of LS mode based devices, electrodes are generally configured on the same surface (e.g., grating electrode is one of the popular layouts) and covered by another friction layer. Then the lateral sliding motion of object on the electrode pattern induces current flow in the external circuit.

For CS mode based control interfaces, various configurations have been investigated for diverse control applications [56–61]. Among them, most devices have the configuration of pressure or tactile sensor array, in order to detect the object motion on the surface. For example, a stretchable triboelectric tactile sensor array with patterned Ag-nanofiber electrodes is reported for trajectory mapping of object, which is further applied as control interface of Pac-Man game [56]. Similarly, another triboelectric sensor array based on water/air-hybrid mechanism is successfully developed as advanced neural interface, achieving selective and force-controlled stimulation of different leg muscles of rats [57]. These sensor array based control interfaces have shown stable output performance and are good for pressure mapping of multiple contacts by simultaneously detecting the output from all the sensor pixels. However, to achieve higher resolution, the number of pixels as well as sensing electrodes needs to be increased dramatically, which induces grand complexity and difficulty in circuitry design and signal processing. To overcome this issue, analogue skin patches with only four edge electrodes are developed [61–64], to detect single contact on the surface once at a time. For each contact motion, the skin patches are able to position the contact location based on the voltage ratios from the two pairs of the opposite electrodes. With advanced grid patterns assembled on top to introduce separation during sliding, detection of sliding trajectory can be achieved [61]. Although sensing electrodes can be reduced to only four through the analogue skin patch design, the output performance is actually not ideal, which has low signal-to-noise ratio and high interference from ambient noise due to the low coupling efficiency of triboelectric charges to the electrodes. Furthermore, the number of electrodes still has great potential be reduced to the ultimate goal of minimalist, i.e., one electrode.

In this regard, LS mode based TENGs with grating electrodes exhibit great potential toward this objective [28,65–72]. TENGs with grating electrode have been investigated for various applications including energy harvesting, sensing, and control interface. For instance, a triboelectric finger bending sensor with grating electrode pattern is presented to monitor the bending motions of a finger and realize quantitative degree/speed control of a robotic hand [72]. Except for the demonstrated 1D robotic finger control, grating structure has great

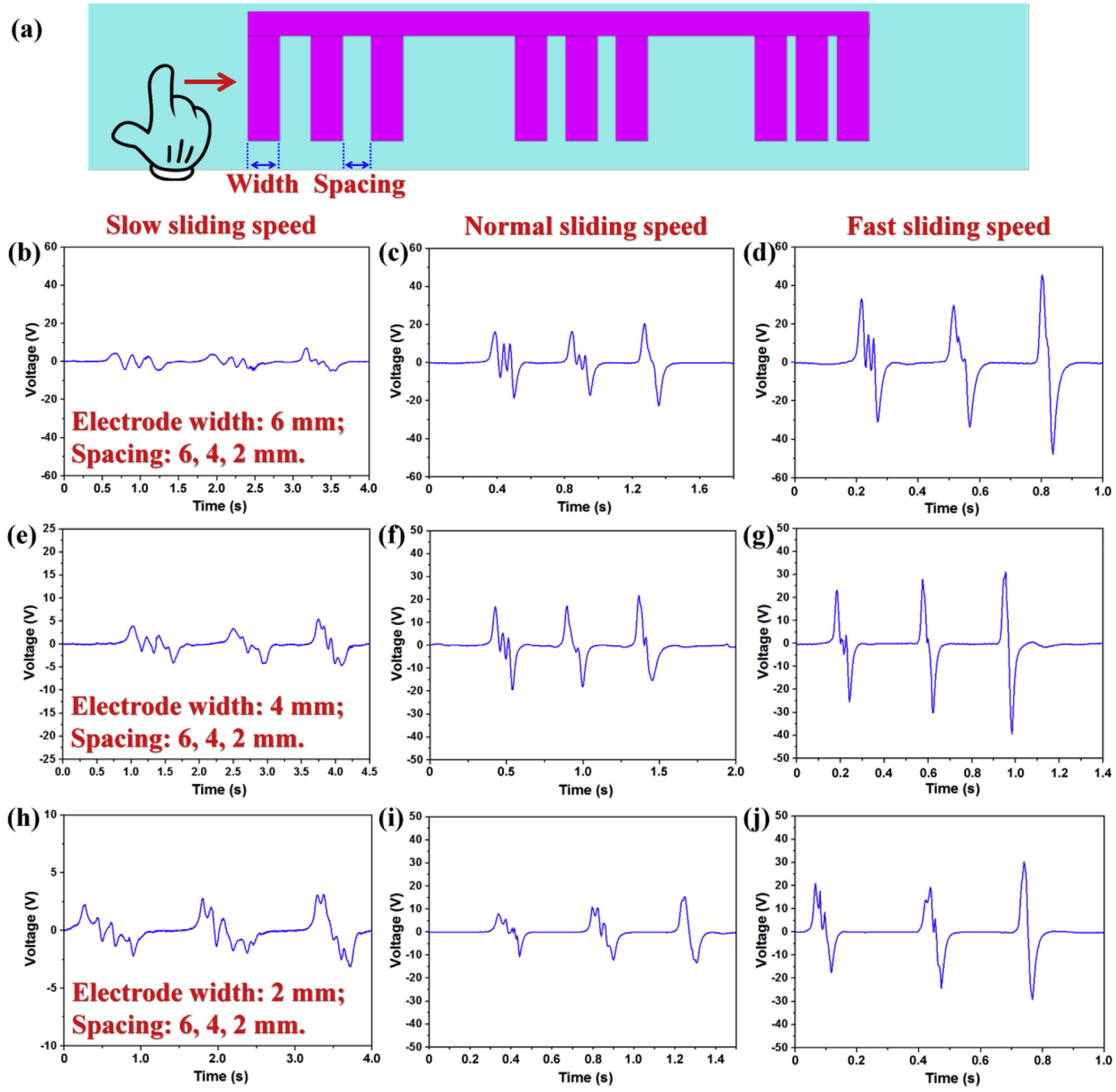

Fig. 2. Optimization of electrode width and spacing. (a) Schematic for the measurement setup. Measurement results with electrode width of 6 mm under (b) slow, (c) normal, and (d) fast sliding speed. Measurement results with electrode width of 4 mm under (e) slow, (f) normal, and (g) fast sliding speed. Measurement results with electrode width of 2 mm under (h) slow, (i) normal, and (j) fast sliding speed.

potential for more advanced control such as 2D and 3D control. In addition to control interfaces, most of the grating TENGs are reported for sensing applications. A triboelectric sensor with grating electrode array along a plastic tube is demonstrated for motion monitoring of a moving object going through the tube [65]. Then a barcode system is proposed for application of personal identification, which is composed of a sliding TENG card with an encoded grating electrode and an uncoded reference electrode on both surfaces, and a reader to detect the information from both electrodes simultaneously [28]. With the help of the reference electrode, the coded information on grating electrode can be decoded by the reader regardless of the sliding speed. Another self-powered motion tracking system is presented based on TENG with grating electrodes of different lengths to differentiate moving direction, moving speed and acceleration [66]. To date, most of the reported grating TENGs are normally demonstrated for 1D application such as motion tracking. Moving forward, to make the most out of the grating structure and realize more advanced control, the grating electrode can be designed into connected 2D layout with different number of electrodes for different directional sensing and controlling. In this way, minimalist control interfaces can be then achieved with only one sensing electrode. Furthermore, since different directions are differentiated through the number of generated output peaks, this minimalist design offers excellent robustness in terms of device reliability even when the ambient parameter changes.

Herein, a single-electrode-output triboelectric control interface is developed with connected grid electrode for multi-directional sensing

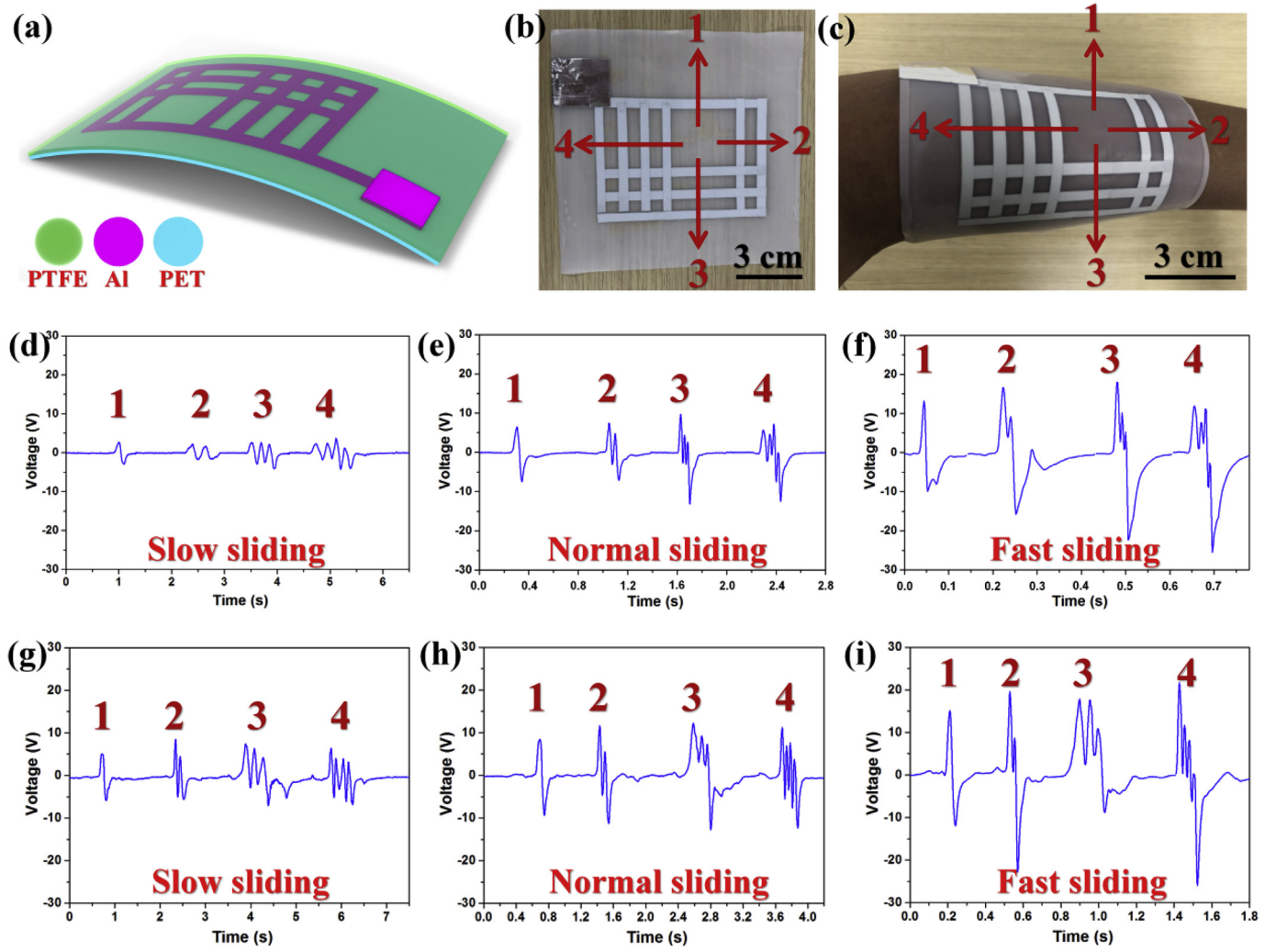

Fig. 3. Characterization of the flexible 2D-control patch. (a) Schematic of the fabricated device. (b) Photograph of the device on a flat table surface. (c) Photograph of the device conformally attached on the surface of human arm. The generated output peaks from the device on table with (d) slow, (e) normal, and (f) fast sliding speed. The generated output peaks from the device on human arm with (g) slow, (h) normal, and (i) fast sliding speed.

and controlling. Compared to other non-triboelectric control interfaces, the developed triboelectric control interface offers various advantages, including self-generated signals, succinct structure, easy fabrication, low cost, and high flexibility. In addition, compared with other triboelectric control interfaces, it shows superiority in several aspects, e.g., realizing multi-directional controlling with only one electrode, detection mechanism irrelevant to the absolute magnitude of output signals (through detecting the number of output peaks), and thereby excellent robustness and reliability in various usage scenarios and for different users. A flexible 2D-control patch with single grid electrode is fabricated to achieve in-plane 2D control. Next, to realize 3D control in free space, a flexible 3D-control card through the integration of two 2D-control patches is developed. Then real-time control of a small vehicle is successfully demonstrated using the control patch (e.g., moving forward/backward, and turning left/right). In addition, 3D virtual drone control in free space is achieved using the control card. The developed flexible, self-powered and minimalist control interfaces show promising applications in various areas such as gaming, virtual/augmented reality, entertainment, smart home, and robotics control, etc.

2. Design and operation mechanism

As illustrated in Fig. 1(a and b), the schematic drawings indicate the detail configurations of the 2D-control patch and the 3D-control card, both of which can be realized on flexible wearable platform. The control patch consists of only three thin layers, i.e., substrate layer of polyethylene terephthalate (PET), electrode layer of grip-pattern Al, and friction layer of polytetrafluoroethylene (PTFE). During the operation, finger is sliding from the middle square across the grating patterns in different directions for the respective direction sensing and controlling. The key concept for multi-directional sensing is the differentiation of outputs in each direction, which can be achieved through distinguishing signal amplitudes, shapes or number of output peaks, etc. Although triboelectric mechanism exhibits good performance in diverse energy harvesting and self-powered sensing applications, its output amplitude and signal shape can be easily affected by the ambient conditions such as humidity and operation manners. On the other hand, using the number of output peaks for differentiation offers a robust and reliable detection mechanism. Therefore, through connecting grating electrodes (with different number for different directions) into one grid pattern, single-electrode triboelectric device can be realized for multi-directional sensing and controlling. Since different number of grating electrodes is adopted for each direction, output signals with different number of output peaks is generated when sliding across each direction, providing a robust and reliable approach for direction differentiation in regardless of ambient humidity, sliding speed, and sliding force, etc. Moreover, combining two control patches, a 3D-control card is developed for 3D object control in free space. Directions

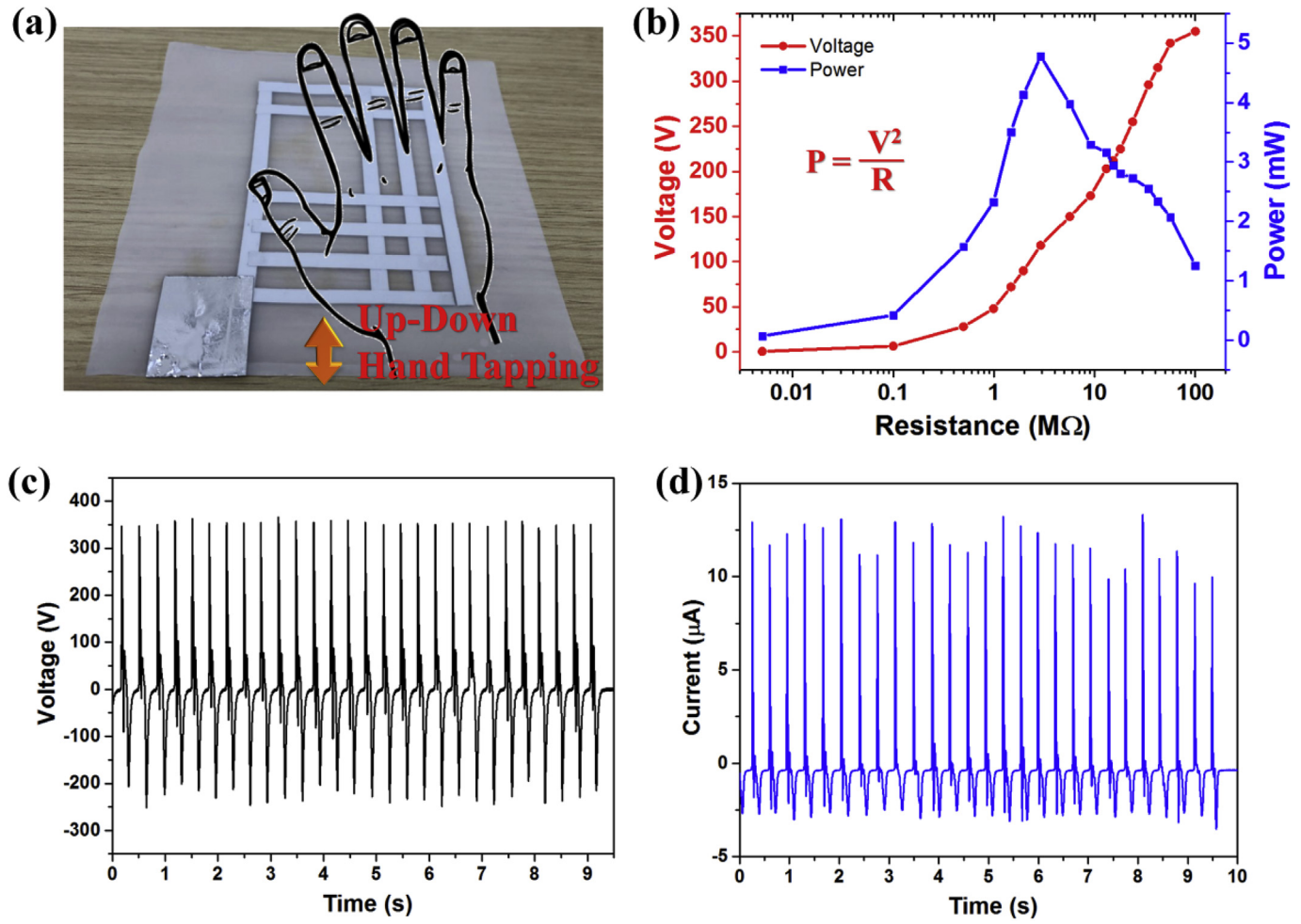

Fig. 4. Energy harvesting performance of the 2D-control patch. (a) Schematic of using the device for scavenging energy from hand tapping. (b) Output voltage and output power on different resistor loads. (c) Output voltage waveform when the device is connected to a 100 MΩ load. (d) Output current waveform of the device under short circuit condition.

of two finger sliding on the opposite surfaces can be detected based on the respective number of output peaks. Through the combination of the two finger motions, six-axis control of object in free space can then be realized, which will be discussed in more details in the next section.

The operation mechanism of the control patch is based on the contact electrification and electrostatic induction between the PTFE friction surface and the sliding object (i.e., human finger wearing nitrile glove), as shown in Fig. 1(c). Here direction with two grating electrodes is taken as an example, where all the grating electrodes are connected to an external resistor load. After finger wearing nitrile glove contacts with PTFE, electrons are injected from the nitrile glove into PTFE at the interface, due to the different electron affinity of the two materials. Thus PTFE surface becomes negatively charged and nitrile glove surface becomes positively charged. Then when finger slides on the first grating electrode, the positive charges on the nitrile glove surface balance the negative charges on the PTFE surface, inducing an electric potential difference. Thus electrons are driven to flow from ground to the first grating electrode, generating a positive output peak on the external circuit. Next, when finger slides out of the first grating electrode, the arisen electric potential difference disappears and electrons flow back to ground, generating a negative output peak on the external circuit. Similarly, when finger slides on and out of the second grating electrode, another output peak (including both the positive peak and the negative peak) is generated. That is, one output signal peak is generated when finger slides across one grating electrode. In this way, different directions with different number of grating electrodes can be differentiated based on the number of generated output peaks, e.g., one output peak will be generated when sliding in the direction with one grating electrode, two output peaks will be generated when sliding in the direction with two grating electrodes, etc.

3. Optimization of electrode with and pitch

Targeting for the control applications using finger (with typical width of ~15 mm) sliding, the width and spacing of the grating electrodes are important parameters in determining the output signal patterns. As depicted in the schematic of Fig. 2(a), three groups of three-electrode pattern are connected together, where the electrode width is the same while the spacing of electrodes are 6 mm, 4 mm and 2 mm for each group. First, electrode width of 6 mm is investigated with finger sliding across all the three groups with a constant speed which is categorized into slow speed (~38.0 mm/s), normal speed (~97.4 mm/s) and fast speed (~152.0 mm/s). The corresponding output signals from these three speeds are illustrated in Fig. 2(b–d). It can be observed that for a constant sliding speed, the output peaks can be differentiated more clearly with larger spacing. If the spacing is too small, multiple output peaks tend to merge into one single peak since the grating electrodes also tend to merge as one. For sliding with different speeds, lower speed generates more separated peaks. If the sliding speed is too fast, multiple output peaks also have the trend to merge into one peak since more output peaks are generated in shorter time duration. Then two other electrode widths (i.e., 4 mm and 2 mm) are investigated with the same

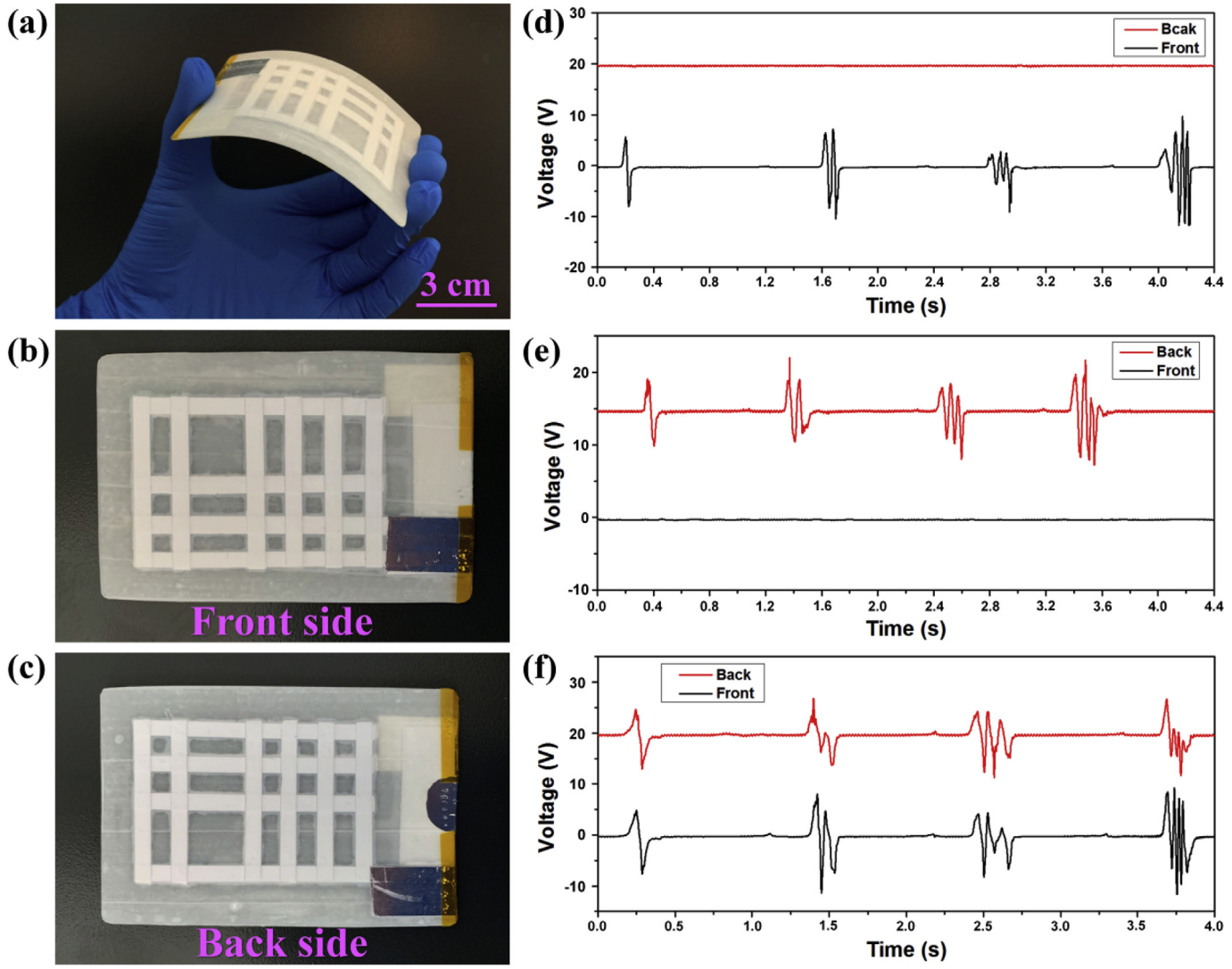

Fig. 5. Characterization of the portable 3D-control card. Photographs showing (a) the bending of the device with fingers, (b) the front side, and (c) the back side of the device. (d) The generated outputs from both electrodes when only sliding on the font side. (e) The generated outputs from both electrodes when only sliding on the back side. (f) The generated outputs from both electrodes when sliding simultaneously on both the font side and the back side.

testing manner in slow, normal and fast sliding speed, as depicted in Fig. 2(e–g) and Fig. 2(h–j). Accordingly, if the electrode width is too small, the output signal peaks may not come out as expected due to the limited contact area of small electrode with finger. Besides, when the spacing of electrodes is too small, all the output peaks may merge into one single peak in a fast sliding speed, inducing difficulty in detecting the accurate output peak number. Therefore, in order to produce output signals with distinguishable peaks, the grating electrodes should have certain width and spacing. Here electrode width of 4 mm and spacing of 6 mm are adopted for both the control patch and the control card.

4. Flexible 2D-control patch

The fabricated flexible 2D-control patch is investigated in terms of output signal generation under different usage scenarios. Fig. 3(a) shows the schematic of the 2D-control patch with three stacking layers of PET substrate, grid Al electrode and PTFE friction layer. Photographs of the flexible patch on table and attached on human arm are depicted in Fig. 3(b and c), showing excellent wearable compatibility for the potential application in wearable electronics. First, the flexible patch is attached on a flat table surface and characterized for the four direction sensing under three different finger sliding speeds (i.e., slow, normal and fast). As illustrated in Fig. 3(d–f), all the output peaks corresponding to the respective directions under sliding can be clearly identified, with sliding speed varying from slow to fast. With the increment of sliding speed, the amplitude of the output signals also increases and the output peaks become closer to each other. Benefited from the peak number based detection mechanism, all the sliding directions can be correctly determined irrelevant of the sliding speed and other ambient parameters, offering excellent robustness and reliability in various usage scenarios and for different users. Next, the flexible patch is attached on human arm and the same characterizations are performed again, as illustrated in Fig. 3(g–i). The measurement results indicate that after attached on human skin, the output peaks from different sliding directions can still be clearly distinguished for all the sliding speeds increasing from slow to fast, once again showing the excellent robustness of the device and its great potentials for the wearable applications.

Except for the use in multi-directional sliding detection and control, the flexible patch can also be adopted for harvesting energy from various human activities such as tapping and sliding. The operation schematic for scavenging energy from hand tapping is shown in Fig. 4(a), with human palm performing periodic contact and separation with the device at a frequency of ~3 Hz. The output voltage and power

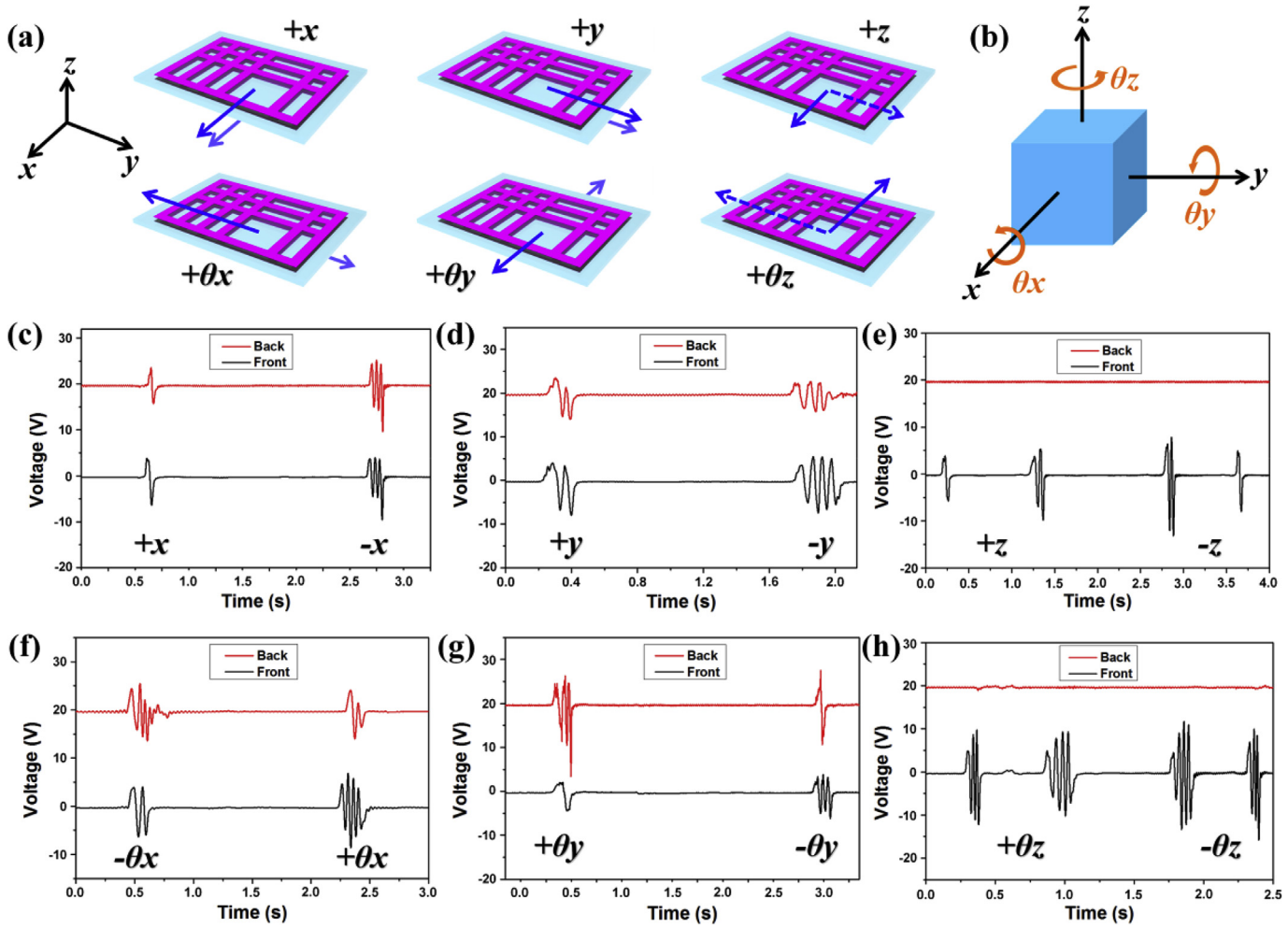

Fig. 6. The 3D control strategy in free space using the 3D-control card. (a) The sliding operations on both surfaces of the device. (b) The corresponding object movements. The output signals from the device for translation movement control in the (c) *x*, (d) *y*, and (e) *z* direction. The output signals from the device for rotation movement control in the (f) *θx*, (g) *θy*, and (h) *θz* direction.

of the device are measured with a series of resistors connected to it as the external load, as depicted in Fig. 4(b). It can be observed that the output voltage of the device increases with the external load resistance, while the output power first increases and then decreases with the external load resistance. The output power of the device reaches a maximum value of 4.8 mW when the external load resistance is 3 MΩ. Fig. 4(c and d) illustrate the recorded output voltage from a 100 MΩ load and the output current in short circuit condition, with the values of ~355 V and ~12 μA, respectively.

5. Portable 3D-control card

Through the integration of two 2D-control patches on both sides of a flexible card, novel 3D control with six degrees of freedom (i.e., *x*, *y*, *z* translation and *θx*, *θy*, *θz* rotation) can be realized. To fabricate the 3D-control card, two 2D-control patches with the same grid electrode pattern are first fabricated. Then a thin PET substrate with a conductive layer of indium tin oxide (ITO) is cut into the same size. The ITO layer serves as a shielding layer of the two individual outputs from the two patches, which eliminates the electrical interference from one electrode to another. Since without the ITO layer, sliding motion on one surface will generate triboelectric outputs on both electrodes due to the electrostatic induction. Next, the two patches are attached on both sides of the ITO/PET substrate. Thus the fabricated 3D-control card has three electrodes, i.e., the front grid-pattern electrode, the back grid-pattern electrode and the middle shielding electrode. During the operation, the shielding electrode is connected to ground and the two other electrodes are connected for output signal measurement. The photographs in Fig. 5(a–c) depict the bending of the 3D-control card with human fingers, top view of its front side and top view of its back side, respectively. The 3D-control card has a similar dimension as the common business cards, which has great portability and can be easily put inside of the pocket. Benefited from the grounded shielding electrode, output signals are generated on the front electrode when sliding on the front side, with no output signals generated from the back electrode, as shown in Fig. 5(d). Similarly, when finger slides on the back side of the card, output signals are also only generated on the back electrode, as indicated in Fig. 5(e). This means that the shielding electrode can effectively eliminate the signal interference between the two electrodes. Fig. 5(f) illustrates the output signals when both sides of the 3D-control card are under sliding motions of two fingers simultaneously toward the same direction. It can be observed that both electrodes exhibit similar output signals for the respective directions.

Due to the grid patterns on both sides, the control card can be applied for the application of 3D control. The detail controlling strategy using the 3D-control card for six degrees of freedom control, i.e., *x*, *y*, *z* translation (forward/backward, up/down, left/right) and *θx*, *θy*, *θz* rotation (yaw, pitch, roll), and the corresponding object movements are illustrated in Fig. 6(a and b), respectively. When both fingers (on the front and the back side) slide toward + *x* (or –*x*) direction, one output peak is (or three output peaks are) generated on both electrodes simultaneously. Through programming, the object then can be made to

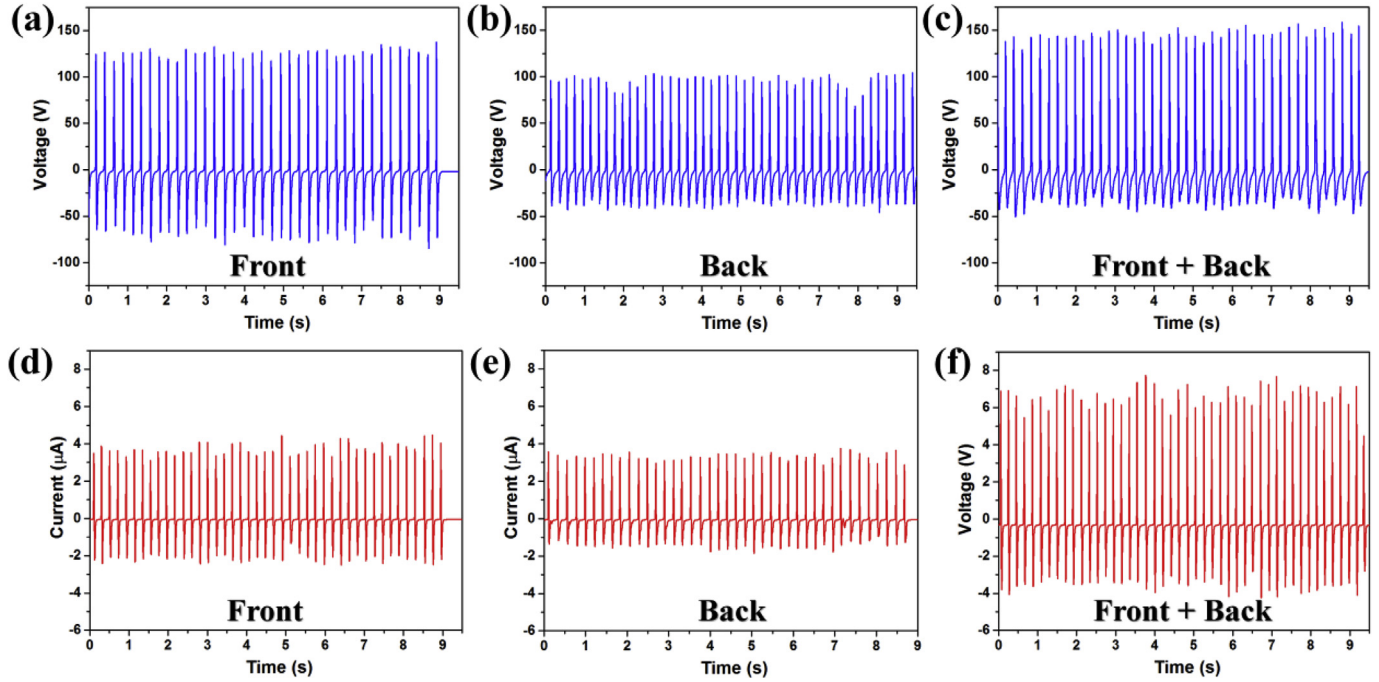

Fig. 7. Energy harvesting performance of the 3D-control card from hand tapping. Output voltages of the device on a 100 MΩ load when tapping on (a) only the front side, (b) only the back side, and (c) both sides. Short circuit currents of the device when tapping on (d) only the front side, (e) only the back side, and (f) both sides.

move in the $+x$ (or $-x$) direction accordingly. Similarly, when both fingers slide toward $+y$ (or $-y$) direction, two output peaks (or four output peaks) are generated on both electrodes. In this way, the object is programmed to move in the $+y$ (or $-y$) direction. In order to control the object to move in the $+z$ (or $-z$) direction, the front finger (on the front side) needs to slide consecutively across $+x$ and then $+y$ (or reversely $+y$ and then $+x$) direction, generating one peak and then two peaks (two peaks and then one peak) on the front electrode. The generated signals from both of the electrodes for the x, y, and z translation control are depicted in Fig. 6(c–e). Then controlling the rotation movement of the object can be realized through moving the two fingers toward the opposite directions. For instance, when the front finger slides toward the $-y$ and the back finger slides toward the $+y$ direction, four output peaks are generated on the front electrode and two output peaks are generated on the back electrode. This controlling motion is an intuitive triggering of the $+\theta x$ rotation, and thus the object is programmed to rotate in the $+\theta x$ direction. For the $-\theta x$ rotation, the front finger needs to slide toward the $+y$ and the back finger needs to slide toward the $-y$ direction. Similarly, when the front finger slides toward the $+x$ and the back finger slides toward the $-x$ direction, one output peak is generated on the front electrode and three output peaks are generated on the back electrode. Accordingly, the object is programmed to rotate in the $+\theta y$ direction. For the $-\theta y$ direction, both fingers need to slide in the opposite directions. To achieve the $+\theta z$ (or $-\theta z$) rotation control, the front finger needs to slide consecutively across $-x$ and then $-y$ (or reversely $-y$ and then $-x$) direction. The generated signals from both of the electrodes for the θx, θy, and θz rotation control are illustrated in Fig. 6(c–e). Therefore, through using the portable 3D-control card and the established controlling strategy, manipulation of an object in 3D free space can be achieved with the sliding motions of two fingers.

The 3D-control card is then investigated in terms of energy harvesting characteristics, as shown in Fig. 7. Both the front side and the back side of the 3D-control card are adopted to scavenge energy from hand tapping. If only the front side is connected in the external circuit, output voltage of 128 V on a 100 MΩ load and short circuit current of 3.7 μA can be achieved, as shown in Fig. 7(a and d). Then if only the back side is connected, the generated output voltage and short circuit current are 100 V and 3.35 μA, as depicted in Fig. 7(b and e). When both the front side and the back side are connected with the external circuit in a parallel manner, a total output of 145 V and 6.85 μA can be achieved from the 3D-control card, as shown in Fig. 7(c and f). It can be observed that the voltage of double-side connection slightly increases and the current is almost twice the value of single-side connection, due to the parallel connection and the resultant decrement of the inner impedance.

6. Demonstrations of 2D/3D control

To show the practical application of the proposed control interfaces, the single-electrode 2D-control patch is first demonstrated to wirelessly control a small vehicle. As presented in Fig. 8(a and b) by the photograph and the block diagram, the entire control system includes the control side and the vehicle side with wireless communication. The control side consists of the self-powered 2D-control patch for control signal generation, processing circuit to convert the signal into square wave, microcontroller unit (MCU) to count the number of generated peaks and then send command signal to the wireless module, and the wireless signal transmitter to communicate with the vehicle side. Power supply is required for the operation of the processing circuit, MCU and wireless transmitter, in order to detect the self-generated voltage signals from the 2D-control patch. In the vehicle side, first the wireless signal receiver will send the received signal from the control side to another MCU, and then the MCU will generate respective signal for the driver circuit to control the movement of the vehicle (i.e., going forward/backward, and turning left/right). Fig. 8(c–f) depict the triboelectric output from the 2D-control patch, the square wave output after the processing circuit, and the photographs of the corresponding vehicle movements for each of the control commands. Due to the parallel connection of the processing circuit mainly composed of a comparator circuit, the overall measurement impedance is decreased compared to the previous measurements, leading to a reduced absolute value in the triboelectric outputs and smaller value variation of output peaks. It can also be observed that the negative peaks of the generated triboelectric signals are less significant. After the processing circuit, the analogue triboelectric outputs are converted into square wave outputs that can be

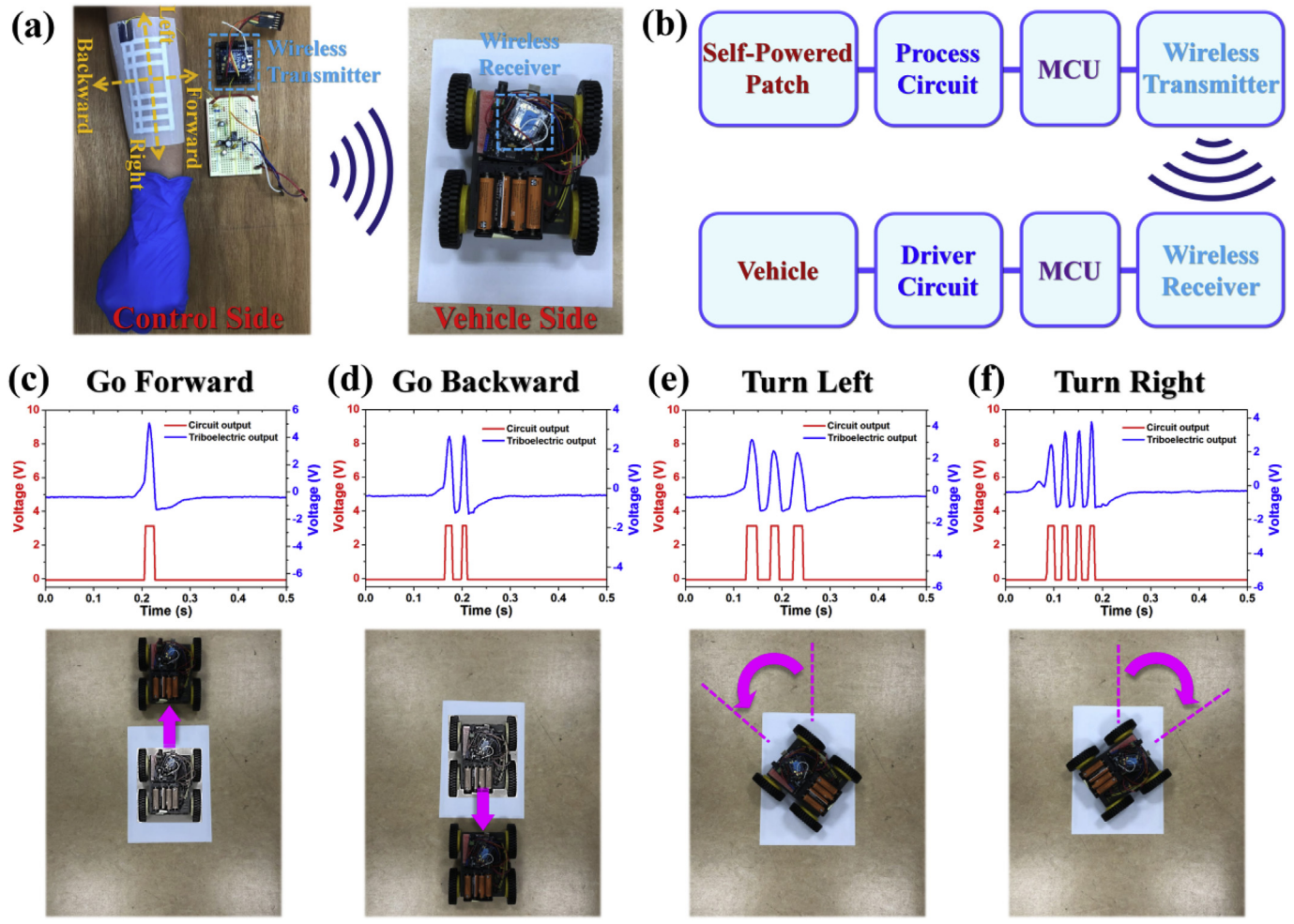

Fig. 8. Demonstration of the 2D-control patch for wireless control of a small vehicle. (a) The photograph and (b) block diagram of the control system. The generated triboelectric outputs from the 2D-control patch, outputs after the processing circuit and the respective control indication of the vehicle for (c) forward control, (d) backward control, (e) left control, and (f) right control.

easily recognized by the MCU. Through counting the number of the output peaks in a certain period, each control command can be clearly identified and send to the control side for vehicle movement control. The video demonstration showing the real-time control of the small vehicle can be found in Supporting Information Video S1.

Supplementary data related to this article can be found online at https://doi.org/10.1016/j.nanoen.2019.03.090

Another demonstration is also conducted using the developed 3D-control card for real-time control of a virtual drone, to showcase the 3D-control capability of the device. As illustrated in Fig. 9(a), the control system consists of the 3D-control card for two-channel control signal generation, processing circuit for triboelectric output to square wave output conversion, MCU for counting the number of output peaks in both channels and sending the corresponding control commands, and computer for generating the respective movements of the drone after receiving the control commands. Fig. 9(b–g) depict the finger operations of the 3D-control card on its two surfaces, the generated signals from the two channels after the processing circuit, and the corresponding movements of the drone in virtual space with six degrees of freedom (up/down, forward/backward, left/right, horizontal left/right rotation, diagonal left/right rotation, and vertical up/down rotation). The recorded video demonstration of the drone control can be found in Supporting Information Video S2, showing the real-time 3D-control capability of the device which can be further applied for other advanced 3D-control applications.

Supplementary data related to this article can be found online at https://doi.org/10.1016/j.nanoen.2019.03.090

7. Conclusions

In summary, two control interfaces based on single-electrode-output design are developed for 2D/3D multi-directional sensing and controlling. This minimalist concept shows superior advantages in practical applications, e.g., realization of multi-directional control using only one electrode that can significantly reduce the complexity of the processing circuitry, signal-amplitude-independent detection mechanism (through detecting the number of generated output peaks), and thus excellent robustness and reliability in various usage scenarios and for different users. The developed flexible 2D-control patch is fabricated with single grid electrode to achieve in-plane 2D control. Meanwhile, the portable 3D-control card is developed to realize 3D control in free space, through the integration of two 2D-control patches. Then the energy harvesting capabilities of both the control patch and the control card are investigated, showing good performance in scavenging energy from hand tapping. Toward real applications, the developed 2D-control patch and the 3D-control card are successfully demonstrated for real-time control of a wireless vehicle (i.e., forward/backward/left/right) and a virtual drone with six degrees of freedom, respectively. The developed flexible, self-powered and minimalist-design control interfaces exhibit promising applications in various areas such as gaming, virtual/augmented reality, entertainment, smart home, and robotics control, etc.

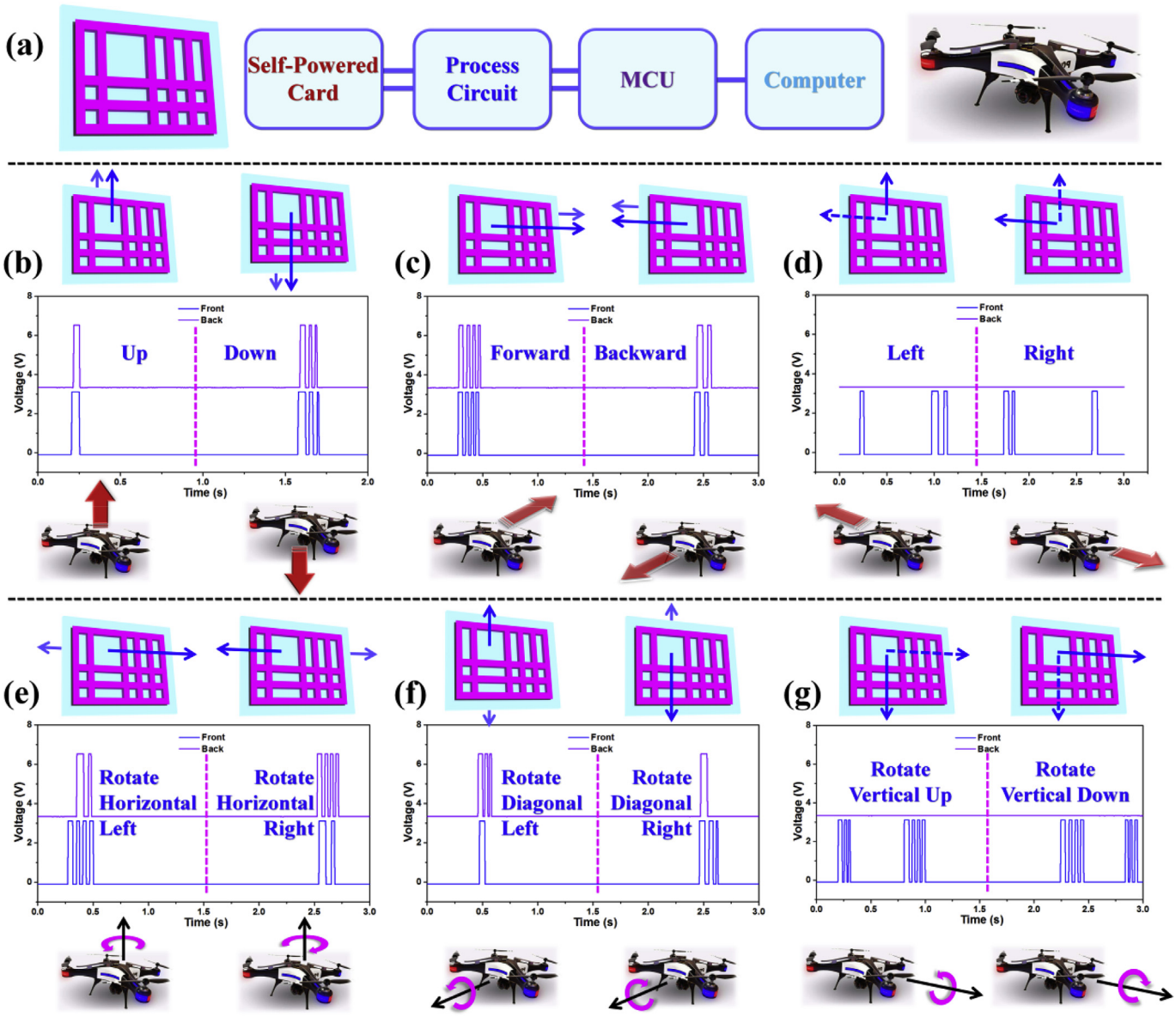

Fig. 9. Demonstration of the 3D-control card for drone control with six degrees of freedom. (a) The block diagram of the control system using the 3D-control card. The finger operations on the two surfaces of the device, the generated signals from the two electrodes after the processing circuit, and the corresponding movements of the drone for (b) up/down control, (c) forward/backward control, (d) left/right control, (e) horizontal left/right rotation control, (f) diagonal left/right rotation control, and (g) vertical up/down rotation control.

Acknowledgement

This work was mainly supported by: HIFES Seed Funding-2017-01 grant (R-263-501-012-133) "*Hybrid Integration of Flexible Power Source and Pressure Sensors*" at the National University of Singapore; and partly supported by the following grants: Singapore-Poland Joint Grant (R-263-000-C91-305) "*Chip-Scale MEMS Micro-Spectrometer for Monitoring Harsh Industrial Gases*" by Agency for Science, Technology and Research (A*STAR), Singapore and NAWA "*Academic International Partnerships of Wroclaw University of Science and technology" programme* by Polish National Agency for Academic Exchange Programme (www.nava.gov.pl); Australian Research Council Future Fellowships Grant (FT130100430); Monash Faculty of Engineering Travel Grant.

References

[1] A. Nordrum, Popular internet of things forecast of 50 billion devices by 2020 is outdated, IEEE Spectr. 18 (2016).
[2] Z. Bao, X. Chen, Flexible and stretchable devices, Adv. Mater. 28 (2016) 4177–4179.
[3] M. Stoppa, A. Chiolerio, Wearable electronics and smart textiles: a critical review, Sensors 14 (2014) 11957–11992.
[4] X. Wang, L. Dong, H. Zhang, R. Yu, C. Pan, Z.L. Wang, Recent progress in electronic skin, Adv. Sci. 2 (2015) 1500169.
[5] T. Wu, F. Wu, J.-M. Redoute, M.R. Yuce, An autonomous wireless body area network implementation towards IoT connected healthcare applications, IEEE Access 5 (2017) 11413–11422.
[6] M. Zhu, Q. Shi, T. He, Z. Yi, Y. Ma, B. Yang, et al., Self-powered and self-functional cotton sock using piezoelectric and triboelectric hybrid mechanism for healthcare and sports monitoring, ACS Nano 13 (2019) 1940–1952.
[7] C. Sun, Q. Shi, D. Hasan, M.S. Yazici, M. Zhu, Y. Ma, et al., Self-powered multi-functional monitoring system using hybrid integrated triboelectric nanogenerators and piezoelectric microsensors, Nano Energy 58 (2019) 612–623.
[8] S. Lee, Q. Shi, C. Lee, From flexible electronics technology in the era of IoT and artificial intelligence toward future implanted body sensor networks, APL Mater. 7 (2019) 031302.
[9] B.C.-K. Tee, A. Chortos, A. Berndt, A.K. Nguyen, A. Tom, A. McGuire, et al., A skin-inspired organic digital mechanoreceptor, Science 350 (2015) 313–316.
[10] H. Fang, K.J. Yu, C. Gloschat, Z. Yang, E. Song, C.-H. Chiang, et al., Capacitively coupled arrays of multiplexed flexible silicon transistors for long-term cardiac electrophysiology, Nat. Biomed. Eng. 1 (2017) 0038.

[11] Y.B. Lee, J.K. Han, S. Noothongkaew, S.K. Kim, W. Song, S. Myung, et al., Toward arbitrary-direction energy harvesting through flexible piezoelectric nanogenerators using perovskite PbTiO3 nanotube Arrays, Adv. Mater. 29 (2017) 1604500.
[12] Q. Shi, T. Wang, T. Kobayashi, C. Lee, Investigation of geometric design in piezoelectric microelectromechanical systems diaphragms for ultrasonic energy harvesting, Appl. Phys. Lett. 108 (2016) 193902.
[13] F.-R. Fan, Z.-Q. Tian, Z.L. Wang, Flexible triboelectric generator, Nano energy 1 (2012) 328–334.
[14] X. Li, G. Xu, X. Xia, J. Fu, L. Huang, Y. Zi, Standardization of triboelectric nanogenerators: progress and perspectives, Nano Energy 56 (2019) 40–55.
[15] Q. Shi, T. He, C. Lee, More than energy harvesting-combining triboelectric nanogenerator and flexible electronics technology for enabling novel micro-/nano-systems, Nano Energy 57 (2019) 851–871.
[16] Z. Liu, Y. Ma, H. Ouyang, B. Shi, N. Li, D. Jiang, et al., Transcatheter self-powered ultrasensitive endocardial pressure sensor, Adv. Funct. Mater. 29 (2018) 1807560.
[17] S.S. Kwak, H.J. Yoon, S.W. Kim, Textile-based triboelectric nanogenerators for self-powered wearable electronics, Adv. Funct. Mater. 29 (2019) 1804533.
[18] Q. Shi, H. Wang, H. Wu, C. Lee, Self-powered triboelectric nanogenerator buoy ball for applications ranging from environment monitoring to water wave energy farm, Nano Energy 40 (2017) 203–213.
[19] Q. Shi, H. Wu, H. Wang, H. Wu, C. Lee, Self-powered gyroscope ball using a triboelectric mechanism, Adv. Energy Mater. 7 (2017) 1701300.
[20] H. Wang, H. Wu, D. Hasan, T. He, Q. Shi, C. Lee, Self-powered dual-mode amenity sensor based on the water–air triboelectric nanogenerator, ACS Nano 11 (2017) 10337–10346.
[21] Y. Hu, Z. Zheng, Progress in textile-based triboelectric nanogenerators for smart fabrics, Nano Energy 56 (2019) 16–24.
[22] H. Chen, Y. Song, X. Cheng, H. Zhang, Self-powered electronic skin based on the triboelectric generator, Nanomater. Energy 56 (2019) 252–268.
[23] B. Shi, Z. Li, Y. Fan, Implantable energy-harvesting devices, Adv. Mater. 30 (2018) 1801511.
[24] H. Feng, C. Zhao, P. Tan, R. Liu, X. Chen, Z. Li, Nanogenerator for biomedical applications, Adv. Healthc. Mater. 7 (2018) 1701298.
[25] P.-K. Yang, Z.-H. Lin, K.C. Pradel, L. Lin, X. Li, X. Wen, et al., Based origami triboelectric nanogenerators and self-powered pressure sensors, ACS Nano 9 (2015) 901–907.
[26] Y.-T. Jao, P.-K. Yang, C.-M. Chiu, Y.-J. Lin, S.-W. Chen, D. Choi, et al., A textile-based triboelectric nanogenerator with humidity-resistant output characteristic and its applications in self-powered healthcare sensors, Nano Energy 50 (2018) 513–520.
[27] Y. Jie, X. Jia, J. Zou, Y. Chen, N. Wang, Z.L. Wang, et al., Natural leaf made triboelectric nanogenerator for harvesting environmental mechanical energy, Adv. Energy Mater. 8 (2018) 1703133.
[28] J. Chen, X. Pu, H. Guo, Q. Tang, L. Feng, X. Wang, et al., A self-powered 2D barcode recognition system based on sliding mode triboelectric nanogenerator for personal identification, Nano Energy 43 (2018) 253–258.
[29] H. Ryu, J.H. Lee, U. Khan, S.S. Kwak, R. Hinchet, S.-W. Kim, Sustainable direct current powering a triboelectric nanogenerator via a novel asymmetrical design, Energy Environ. Sci. 11 (2018) 2057–2063.
[30] R. Wang, S. Gao, Z. Yang, Y. Li, W. Chen, B. Wu, et al., Engineered and laser-processed chitosan biopolymers for sustainable and biodegradable triboelectric power generation, Adv. Mater. 30 (2018) 1706267.
[31] T. He, Q. Shi, H. Wang, F. Wen, T. Chen, J. Ouyang, et al., Beyond energy harvesting-multi-functional triboelectric nanosensors on A textile, Nano Energy 57 (2018) 338–352.
[32] K.H. Koh, Q. Shi, S. Cao, D. Ma, H.Y. Tan, Z. Guo, et al., A self-powered 3D activity inertial sensor using hybrid sensing mechanisms, Nano Energy 56 (2019) 651–661.
[33] Z.L. Wang, T. Jiang, L. Xu, Toward the blue energy dream by triboelectric nanogenerator networks, Nano Energy 39 (2017) 9–23.
[34] B. Shi, Z. Li, Y. Fan, Implantable energy-harvesting devices, Adv. Mater. 30 (2018) 1801511.
[35] B. Chen, Y. Yang, Z.L. Wang, Scavenging wind energy by triboelectric nanogenerators, Adv. Energy Mater. 8 (2018) 1702649.
[36] L. Chen, Q. Shi, Y. Sun, T. Nguyen, C. Lee, S. Soh, Controlling surface charge generated by contact electrification: strategies and applications, Adv. Mater. 30 (2018) 1802405.
[37] W. Yang, X. Wang, H. Li, J. Wu, Y. Hu, Z. Li, et al., Fundamental research on the effective contact area of micro-/nano-textured surface in triboelectric nanogenerator, Nano Energy 57 (2018) 41–47.
[38] D. Yoo, S.-C. Park, S. Lee, J.-Y. Sim, I. Song, D. Choi, et al., Biomimetic anti-reflective triboelectric nanogenerator for concurrent harvesting of solar and raindrop energies, Nano Energy 57 (2018) 424–431.
[39] P. Cheng, H. Guo, Z. Wen, C. Zhang, X. Yin, X. Li, et al., Largely enhanced triboelectric nanogenerator for efficient harvesting of water wave energy by soft contacted structure, Nano Energy 57 (2018) 432–439.
[40] K. Shi, X. Huang, B. Sun, Z. Wu, J. He, P. Jiang, Cellulose/BaTiO3 aerogel paper based flexible piezoelectric nanogenerators and the electric coupling with triboelectricity, Nano Energy 57 (2018) 450–458.
[41] C. Zhao, Q. Zhang, W. Zhang, X. Du, Y. Zhang, S. Gong, et al., Hybrid piezo/triboelectric nanogenerator for highly efficient and stable rotation energy harvesting, Nano Energy 57 (2018) 440–449.
[42] F. Chen, Y. Wu, Z. Ding, X. Xia, S. Li, H. Zheng, et al., A novel triboelectric nanogenerator based on electrospun polyvinylidene fluoride nanofibers for effective acoustic energy harvesting and self-powered multifunctional sensing, Nano Energy 56 (2019) 241–251.
[43] H.-J. Yoon, H. Ryu, S.-W. Kim, Sustainable powering triboelectric nanogenerators: approaches and the path towards efficient use, Nano energy 51 (2018) 270–285.
[44] S. Lee, R. Hinchet, Y. Lee, Y. Yang, Z.H. Lin, G. Ardila, et al., Ultrathin nanogenerators as self-powered/active skin sensors for tracking eye ball motion, Adv. Funct. Mater. 24 (2014) 1163–1168.
[45] Z.H. Lin, G. Cheng, Y. Yang, Y.S. Zhou, S. Lee, Z.L. Wang, Triboelectric nanogenerator as an active UV photodetector, Adv. Funct. Mater. 24 (2014) 2810–2816.
[46] Z.H. Lin, G. Zhu, Y.S. Zhou, Y. Yang, P. Bai, J. Chen, et al., A self-powered triboelectric nanosensor for mercury ion detection, Angew. Chem. 125 (2013) 5169–5173.
[47] Y. Yang, Y.S. Zhou, H. Zhang, Y. Liu, S. Lee, Z.L. Wang, A single-electrode based triboelectric nanogenerator as self-powered tracking system, Adv. Mater. 25 (2013) 6594–6601.
[48] Y. Yang, H. Zhang, R. Liu, X. Wen, T.C. Hou, Z.L. Wang, Fully enclosed triboelectric nanogenerators for applications in water and harsh environments, Adv. Energy Mater. 3 (2013) 1563–1568.
[49] S. Lee, Y. Lee, D. Kim, Y. Yang, L. Lin, Z.-H. Lin, et al., Triboelectric nanogenerator for harvesting pendulum oscillation energy, Nano Energy 2 (2013) 1113–1120.
[50] S. Wang, X. Wang, Z.L. Wang, Y. Yang, Efficient scavenging of solar and wind energies in a smart city, ACS Nano 10 (2016) 5696–5700.
[51] Y. Wu, X. Zhong, X. Wang, Y. Yang, Z.L. Wang, Hybrid energy cell for simultaneously harvesting wind, solar, and chemical energies, Nano Res. 7 (2014) 1631–1639.
[52] Y. Wu, X. Wang, Y. Yang, Z.L. Wang, Hybrid energy cell for harvesting mechanical energy from one motion using two approaches, Nano Energy 11 (2015) 162–170.
[53] T. Quan, X. Wang, Z.L. Wang, Y. Yang, Hybridized electromagnetic–triboelectric nanogenerator for a self-powered electronic watch, ACS Nano 9 (2015) 12301–12310.
[54] H. Guo, X. Pu, J. Chen, Y. Meng, M.-H. Yeh, G. Liu, et al., A highly sensitive, self-powered triboelectric auditory sensor for social robotics and hearing aids, Sci. Robot. 3 (2018) eaat2516.
[55] J. Shao, T. Jiang, W. Tang, L. Xu, T.W. Kim, C. Wu, et al., Studying about applied force and the output performance of sliding-mode triboelectric nanogenerators, Nano Energy 48 (2018) 292–300.
[56] X. Wang, Y. Zhang, X. Zhang, Z. Huo, X. Li, M. Que, et al., A highly stretchable transparent self-powered triboelectric tactile sensor with metallized nanofibers for wearable electronics, Adv. Mater. 30 (2018) 1706738.
[57] S. Lee, H. Wang, J. Wang, Q. Shi, S.-C. Yen, N.V. Thakor, et al., Battery-free neuromodulator for peripheral nerve direct stimulation, Nano Energy 50 (2018) 148–158.
[58] T. Chen, M. Zhao, Q. Shi, Z. Yang, H. Liu, L. Sun, et al., Novel augmented reality interface using a self-powered triboelectric based virtual reality 3D-control sensor, Nano Energy 51 (2018) 162–172.
[59] T. Chen, Q. Shi, Z. Yang, J. Liu, H. Liu, L. Sun, et al., A self-powered six-Axis tactile sensor by using triboelectric mechanism, Nanomaterials 8 (2018) 503.
[60] H. Wu, Q. Shi, F. Wang, A.V.Y. Thean, C. Lee, Self-powered cursor using a triboelectric mechanism, Small Methods 2 (2018) 1800078.
[61] T. Chen, Q. Shi, M. Zhu, T. He, L. Sun, L. Yang, et al., Triboelectric self-powered wearable flexible patch as 3D motion control interface for robotic manipulator, ACS Nano 12 (2018) 11561–11571.
[62] T. Chen, Q. Shi, K. Li, Z. Yang, H. Liu, L. Sun, et al., Investigation of position sensing and energy harvesting of a flexible triboelectric touch pad, Nanomaterials 8 (2018) 613.
[63] T. Li, J. Zou, F. Xing, M. Zhang, X. Cao, N. Wang, et al., From dual-mode triboelectric nanogenerator to smart tactile sensor: a multiplexing design, ACS Nano 11 (2017) 3950–3956.
[64] M. Shi, J. Zhang, H. Chen, M. Han, S.A. Shankaregowda, Z. Su, et al., Self-powered analogue smart skin, ACS Nano 10 (2016) 4083–4091.
[65] Y. Su, G. Zhu, W. Yang, J. Yang, J. Chen, Q. Jing, et al., Triboelectric sensor for self-powered tracking of object motion inside tubing, ACS Nano 8 (2014) 3843–3850.
[66] M. Chen, X. Li, L. Lin, W. Du, X. Han, J. Zhu, et al., Triboelectric nanogenerators as a self-powered motion tracking system, Adv. Funct. Mater. 24 (2014) 5059–5066.
[67] Y. Xie, S. Wang, S. Niu, L. Lin, Q. Jing, J. Yang, et al., Grating-structured free-standing triboelectric-layer nanogenerator for harvesting mechanical energy at 85% total conversion efficiency, Adv. Mater. 26 (2014) 6599–6607.
[68] Q. Jing, Y. Xie, G. Zhu, R.P. Han, Z.L. Wang, Self-powered thin-film motion vector sensor, Nat. Commun. 6 (2015) 8031.
[69] Z. Su, H. Wu, H. Chen, H. Guo, X. Cheng, Y. Song, et al., Digitalized self-powered strain gauge for static and dynamic measurement, Nano Energy 42 (2017) 129–137.
[70] S.Y. Kuang, G. Zhu, Z.L. Wang, Triboelectrification-enabled self-powered data storage, Adv. Sci. 5 (2018) 1700658.
[71] Z. Yuan, X. Du, N. Li, Y. Yin, R. Cao, X. Zhang, et al., Triboelectric-based transparent secret code, Adv. Sci. 5 (2018) 1700881.
[72] X. Pu, H. Guo, Q. Tang, J. Chen, L. Feng, G. Liu, et al., Rotation sensing and gesture control of a robot joint via triboelectric quantization sensor, Nano Energy 54 (2018) 453–460.

Qiongfeng Shi received his B.Eng. degree from the Department of Electronic Engineering and Information Science, University of Science and Technology of China (USTC) in 2012, and received his Ph.D. degree from the Department of Electrical and Computer Engineering, National University of Singapore (NUS) in 2018. He is currently a Research Fellow in the Department of Electrical and Computer Engineering, National University of Singapore. His research interests include energy harvesters, triboelectric nanogenerators, self-powered sensors, and wearable/implantable electronics.

Chunkai Qiu received the B.Eng. degree from Monash University, Australia in 2017. He is currently pursuing the Ph.D. degree in the Department of Electrical and Computer Systems Engineering, Monash University, Australia. His main area of research interest is wearable devices and triboelectric nanogenerator.

Tianyiyi He received her B.Eng. degree from the School of Microelectronics and Solid-state Electronics at the University of Electronic Science and Technology of China (UESTC), Chengdu, China, in 2016. She is now a Ph.D. candidate in the Department of Electrical and Computer Engineering, National University of Singapore. Her research interests focus mainly on thermoelectrics.

Fan Wu received the B.Eng. degree from Monash University in 2015, where he is currently pursuing the Ph.D. degree in electrical and computer systems engineering. He was a Research Assistant with the Engineering Department from 2015 to 2017. His main areas of research interest are wireless sensor network, wearable sensors, energy harvesting, triboelectric nanogenerator, and IoT innovations.

Minglu Zhu received his B.Bus. degree in Business Administration from the School of Business at State University of Bangladesh, Dhaka, Bangladesh, in 2010, and B.Sc. degree in Materials Science and Engineering from the School of Materials Science and Engineering at University of Illinois at Urbana-Champaign, Illinois, United States, in 2014. He is now a Ph.D. student at the Department of Electrical & Computer Engineering, NUS. His research interests focus mainly on MEMS based energy harvesters and self-powered sensors.

Jan A. Dziuban, Prof., well recognized specialist in microsystem technology and applications. Author of over 200 publications concerning microsystem and vacuum nanoelectronics. One of the fathers of R&D activities in microsystem techniques in Poland.

Rafał Walczak, Prof. of WUST, Head of the Department of Microengineering and Photovoltaics of Faculty of Microsystem Electronics and Photonics of Wrocław University of Technology (WUST). Author of over 150 publications in the field of microsystems, analytical microsystems for life-science applications and 3D printed microsystems. He is now leader of the group (www.memslab.eu) working on applicability of 3D printing techniques for fabrication of microfluidic devices, sensors and MEMS.

Mehmet Rasit Yuce is an associate professor in the Department of Electrical and Computer Systems Engineering, Monash University, Australia. He received the Ph.D. degree in Electrical and Computer Engineering from North Carolina State University (NCSU). His research interests include wearable devices, Internet-of-Things for healthcare, wireless implantable telemetry, wireless body area network, bio-sensors, integrated circuit technology dealing with digital, analogue and radio frequency circuit designs. He received a NASA group achievement award in 2007. He is a topical editor for IEEE Sensors Journal, an editor-in-chief for Sensors, and a guest editor for IEEE Journal of Biomedical and Health Informatics in 2015.

Chengkuo Lee received his Ph.D. degree in Precision engineering from The University of Tokyo in 1996. Currently, he is the director of Center for Intelligent Sensors and MEMS, and an Associate Professor in the Department of Electrical and Computer Engineering, National University of Singapore, Singapore. In 2001, he cofounded Asia Pacific Microsystems, Inc., where he was the Vice President. From 2006 to 2009, he was a Senior Member of the Technical Staff at the Institute of Microelectronics, A-STAR, Singapore. He has contributed to more than 300 international conference papers and extended abstracts and 280 peer-reviewed international journal articles.